EasyChair Preprint

№ 9816

Size Measurement of Stone Images Based on Improved UNet

Ning Chen, Xinkai Ma, Jun Peng, Shangzhu Jin, Xiao Wu, Yan Wu and Haixia Luo

March 2, 2023

Size Measurement of Stone Images Based on Improved UNet

Ning Chen*, Xinkai Ma, Jun Peng, Shangzhu Jin, Xiao Wu, Yan Wu, Haixia Luo
College of Intelligent Technology and Engineering
Chongqing University of Science and Technology, Chongqing 401331, China
E-mail: chenning@cqust.edu.cn; irvingmxk@cqust.edu.cn
*Corresponding author

***Abstract*—To address the current problem of calculating stone grain size in the field of sand and gravel aggreg es, image segmentation of stone targets is achieved by stone images, and the grain length of stone targets is finally obtained. By pre-processing the target stone images, the pre-processed stone images are segmented and predicted using deep learning image processing techniques, and the predicted result maps are subjected to morphological and image binarization operations for subsequent stone particle size calculation. The algorithm is implemented to delineate the assignment of individual stone regions and to find the boundary coordinate points of individual stone image regions, and to calculate the image grain size length of stones from them. The true grain length of the stone is calculated by the proportional mapping relationship between the camera and the pixel length of the stone taken and the real stone length. Through experiments, this operation procedure can segment and calculate the grain length of stones quickly and accurately.**

***Index Terms*—stone; grain size measurement; semantic segmentation; mapping**

I. Introduction

Sand and gravel aggregate is one of the important raw materials in the infrastructure construction industry, playing an important role in projects such as housing, highway and bridge construction. According to the actual needs of engineering projects, the stone industry uses large machinery and equipment such as stone crushers to crush and process large size and irregular rocks into stones of different sizes to meet the different needs of stone materials for engineering and other projects.

Size of different stone, China set the stone division standards, according to the different grain size, divided into stone and sand, for stone and sand, in the field of taxation and taxation, the implementation of different taxation standards. At present, the main problem in the process of stone taxation is to measure the length of stone particle size for a batch of stone.

At present, the traditional stone particle size measurement method is through workers, manual sampling for stone particle size detection, manual sampling workload is large, tedious work, manual measurement of stone particle size is time-consuming and labor-intensive, the measurement data is not accurate, the data record keeping is cumbersome. Moreover, the irregular shape of the stones does not allow accurate measurement of the required length, and the rough surface of the stones can easily damage the precision measuring tools and equipment, while the manual sampling can only reflect the length of the particle size of a small portion of the stones. In addition, manual sampling also has a large randomness, can not reflect the average particle length of the current batch of sand and gravel aggregates.

Another method is screening by industrial stone sieving machines. When using this method, the stones can only be divided at the crushing stage, and the results obtained are coarser, and only stones in a certain particle size range can be obtained, and the exact particle length of stone particle size in sand and gravel aggregates cannot be obtained.

In response to a series of problems in the sand and gravel aggregate industry, computer vision solutions have emerged. By means of an externally erected webcam, the stone target to be detected can be photographed, and the stone image can be segmented by semantic segmentation technology, and finally the particle size length of the stone can be calculated according to the mapping scale factor of the distance between the camera and the photographed stone target. This method, which does not require manual sampling of stones, greatly simplifies the operation steps of workers by means of computer processing, and can more accurately obtain the average particle length of stone targets in the current test sand and gravel aggregates.

The main traditional image segmentation methods are threshold-based segmentation methods [1], region-based segmentation methods [2], and edge-based segmentation methods [3]. The traditional image segmentation methods can be applied to the common segmentation task of common large-area images in which only a single major object exists alone or in the image. For the segmentation of stones proposed in this paper, there are the following problems, close connection between stone targets in the same image, blurred background and adhesion, etc. The traditional image segmentation methods cannot solve the segmentation task of this type of image better.

In order to solve the above problems, this paper uses an improved UNet network for segmentation of stone images from a deep learning perspective to obtain better segmentation results. At present, in the field of deep learning, the deep learning networks for image segmentation are mainly the full convolutional network FCN [4] based on semantic segmentation, UNet [5] network developed on the basis of full convolutional network, PSPNet [6] network, DeeplabV3+ [7]

network, etc. As shown in the figure 1, the effect of semantic segmentation is illustrated.

Fig. 1. Schematic diagram of the effect of semantic segmentation

Convolutional neural networks (CNN) [8] are capable of classifying images, while fully convolutional networks (FCN) can perform pixel-level segmentation tasks on images, solving the problem of semantic-level image segmentation tasks [4]. The traditional convolutional network (CNN) connects several fully connected layers after several convolutional layers, which are used to map the feature information extracted from several previous convolutional layers into a fixed-length feature vector, and perform the image classification task according to the different vector information. And the fully convolutional network replaces the fully connected layers, which are connected after the convolutional network, with convolutional layers, so it is called a fully convolutional network.

The output of the full convolutional network is a picture that is completed with a classification label based on different pixel points. In addition to the problem of the fully connected layer, another problem of semantic segmentation using convolutional neural networks is the pooling layer [9]. Any kind of pooling operation leads to the loss of information at the pixel locations of the image, but the greatest requirement for semantic segmentation is to preserve the information at the pixel locations. To solve this realistic problem, driven by the medical field, UNet networks were created, UNet networks, the general structure of which resembles the letter U. A UNet consists of an encoder (downsampler) and a decoder (upsampler).

In this paper, by improving the original UNet network to segment the stone targets, we can segment the stone targets well and get each independent stone target, and finally the real particle size calculation of the stone is performed according to the stone effect map after the neural network processing.

II. General description of the methodological process

The final requirement of this paper is to obtain the actual average particle length of all segmented gravel targets in the actual captured gravel images[23]. Before calculating the actual length of the gravel particle size, the first preparation work is to segment the gravel targets more accurately. Based on the above experimental requirements, the overall experimental steps are divided into two stages: stone image segmentation and stone particle size calculation.

For the process of stone segmentation, the stone segmentation network model is constructed first [22]. Before the model training starts, it is necessary to construct the stone dataset by selecting the original images of stones that meet the specification of the shooting place and getting the standard images of sand and stone edges by manually annotating the sand and stone edges as the stone dataset. The figure shows the captured gravel images and the annotated generated gravel images.

The stone dataset, in the ratio of 8:2, is randomly divided into a training set test set. The stone segmentation model is obtained by training the network model.

In the stone segmentation prediction stage, after cropping the original stone image to the size required by the network, the predicted stone image, after morphological processing and image binarization, is passed through the stone segmentation model to obtain the segmentation result image of the stone[21].

For the stone particle size length calculation stage, for the segmented result image of the stone obtained, the lateral and longitudinal pixel particle size lengths of each stone target after segmentation are calculated and averaged as the average lateral and longitudinal pixel particle size lengths of the stone image, and finally the larger value of the lateral or longitudinal particle size length is selected as the average particle size length of the stone in the current image. In the process of mapping the true particle size length of stones, the true particle size length of stones is mapped by the particle size length of stones in the image. The general flow of stone image particle size detection is shown in Figure 2.

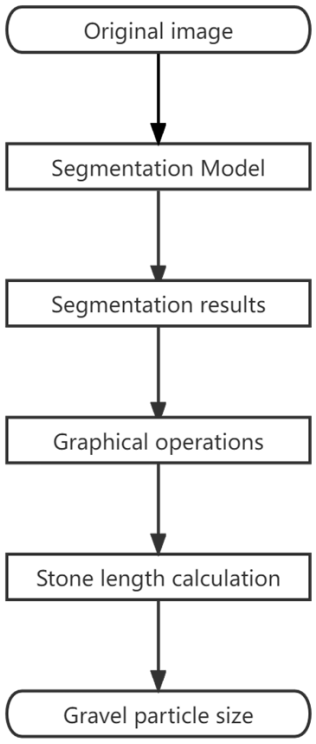

Fig. 2. Stone particle size measurement method process

III. Stone Target Segmentation

A. Neural Network Architecture

Before performing the stone particle length calculation, the individual stone targets need to be segmented [16]. In this paper, a modified UNet network structure is used for the independent stone sub-target segmentation task. It mainly consists of three parts, the first part is the backbone feature extraction part, the second part is the enhanced feature extraction part, and the third part is the prediction part.

The first part of the neural network is the backbone feature extraction part, and several feature layers can be obtained using the backbone part. The backbone feature extraction part of UNet is similar to the VGG [10] network architecture, both of which are a stacked combination of convolutional layers and maximum pooling layers. Five initial effective feature layers can be obtained by using the backbone feature extraction part, and the five effective feature layers extracted can be used for feature fusion operation in the second step of enhanced feature extraction.

The backbone feature extraction network used in this paper is VGG16, which can easily use the pre-trained weights on ImageNet. Only two types of layers are used to use VGG16 as the backbone feature extraction network, which are convolutional layer and maximum pooling layer. A schematic of the VGG16 network is shown in Fig 3.

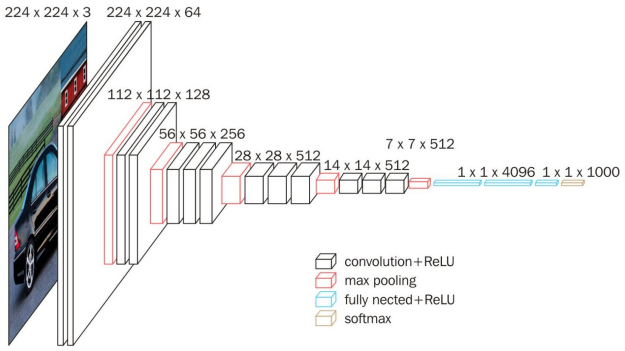

Fig. 3. VGG16 network architecture diagram

The second part of the neural network is the enhanced feature extraction part, which can use the five initial effective feature layers obtained from the backbone part to upsample and perform feature fusion to obtain a final, effective feature layer that incorporates all the features.

The feature fusion is done by up-sampling and stacking the feature layers[11]. In order to build a neural network with better generality, the original UNet network is based on the up-sampling process with double up-sampling and then feature fusion, and the final feature layer is obtained with the same height and width as the input image.

The third part of the neural network is the prediction part, which uses the last effective feature layer obtained to classify each feature point, which is equivalent to classifying each pixel point, and finally using the features to obtain prediction results[12]. The original architecture of the UNet network is shown in Figure 4.

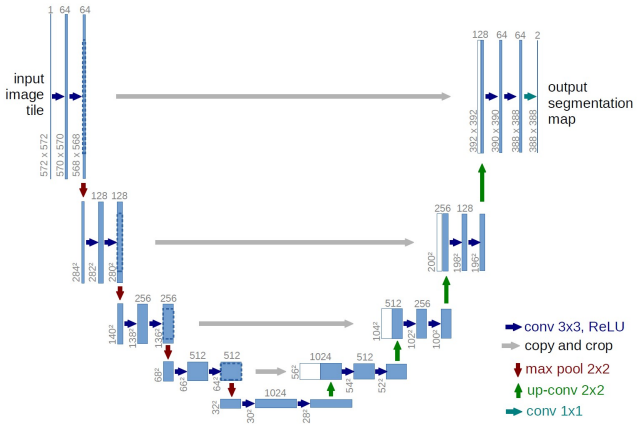

Fig. 4. Architecture diagram of UNet network

B. Loss Explanation

The Loss used in this paper consists of two parts.

- Cross Entropy Loss
- Dice Loss

Cross Entropy Loss [17] is the cross entropy loss, which is used when the semantic segmentation platform uses Softmax to classify the pixel points.

Dice loss [18] takes the evaluation index of semantic segmentation as Loss, and Dice coefficient is an ensemble similarity measure function, which is usually used to calculate the similarity of two samples and takes values in the range of [0,1].

$$S = \frac{2|X \cap Y|}{|X| + |Y|} \tag{1}$$

As in Equation 1, the value of s is the ratio of the value of the cross product of 2 times the predicted result and the true result to the value of the predicted result and the true result. Its value is between 0 and 1. The larger the value, the greater the overlap between the predicted and true results.

C. Network Training

The stone-image datasets used in this experiment are all webcam acquisitions with 40 stone-images, which are manually labeled and randomly divided according to the ratio of 8:2 for the training set test set.

The parameters used for training, Num_Classes is the pixel classification category, Freeze_Epoch is the number of freeze training, Freeze_Batch_Size is the batch size during freeze training, the backbone of the model is frozen during freeze training and the feature extraction network does not change. unFreeze_Epoch is the number of unfreeze training. UnFreeze_Batch_Size is the batch size at the time of unfreeze training, the backbone of the model is not frozen at the time of unfreeze training, the UnFreeze_Batch_Size is 4 at the time of unfreeze training, and the feature extraction network is

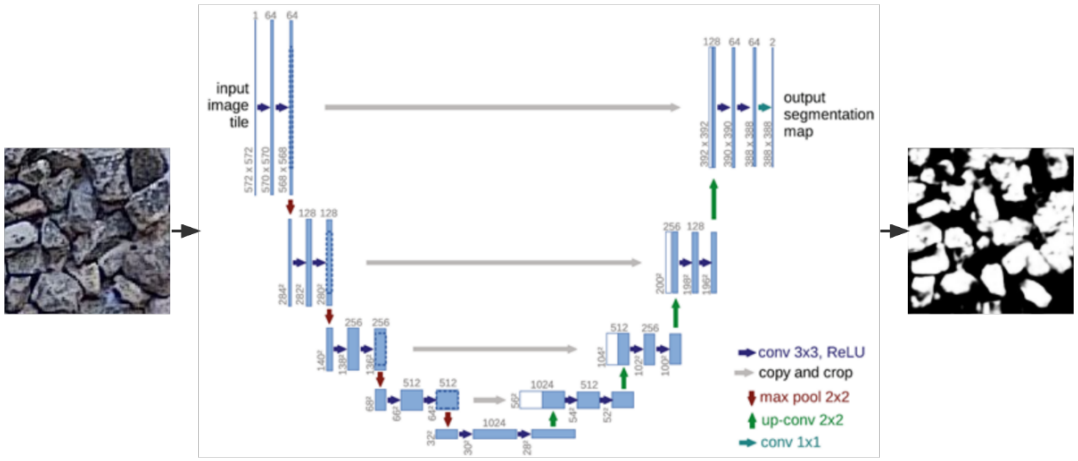

Fig. 5. Structure diagram of stone target segmentation model

changed. The optimizer used for network training is Adam optimizer, and the Momentum parameter used inside the optimizer is 0.9. Since Adam causes weight_decay error, the weight decay weight_decay parameter is 0. Figure 5 shows the process of model prediction.

For the details of the training parameters configuration of the network, as shown in Table 1.

TABLE I
NETWORK TRAINING PARAMETERS TABLE

Training parameters	Parameter Value
Num_Classes	2
Freeze_Epoch	50
Freeze_Batch_Size	8
UnFreeze_Epoch	150
UnFreeze_Batch_Size	4
Optimizer_Type	adam
Momentum	0.9
Weight_Decay	0

IV. CALCULATION OF THE LONGEST PARTICLE SIZE OF THE STONE TARGET

A. Stone division

After the original image has been predicted by the model to obtain the final result image (binarized image), the second part of the experiment is to calculate the average particle length of the stone target[19].

For the segmented result, all pixel coordinates of each stone in the binarized image are obtained, and the first traversal of each pixel in said binarized image is performed in turn, and each pixel in said binarized image is marked $min(label_{n(x,y)})$, that is, the smallest $label$ of the midpoint of its neighborhood.If a different $label$ is found in the neighborhood, put the $label$, into a set S_i, the $label$ of each connected domain C_i in the same set, $label_{(x,y)} \in S_i$, $(x, y) \in C_i$.

A second traversal of each pixel in said binarized image in turn, updating the $label$ of each pixel point to its smallest $label$ for the set, $label_{(x,y)} = \min(S_i)$, $(x, y) \in C_i$.

For the said binarized image after two traversal operations, each non-linked individual stone image region is delineated, where each individual region has an independent pixel label to facilitate subsequent stone pixel grain length calculation. Figure 6 shows the schematic diagram to determine whether the image is a connected domain.

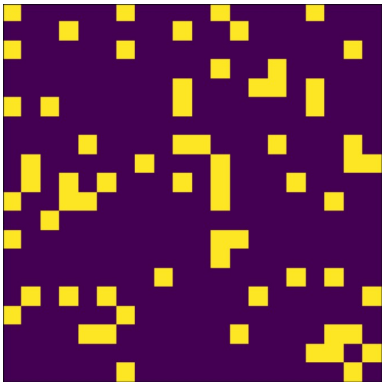

Fig. 6. Image connectivity domain schematic

B. Calculation of stone particle size

Find the boundary coordinate index based on said area image and calculate the pixel grain diameter length of each stone to get the pixel length of the stone[20].

Obtain the scale mapping relationship between the real stone grain length and the stone pixel grain length based on the lens distance to photograph the stone length. The pixel length of the stone is mapped to the real stone grain length by the measured scale factor.

Based on all the index positions saved in the stone division stage, all the index positions of the top, bottom, left and right 4 boundary coordinates are searched for the coordinate points of the same marked pixel. Based on the four boundary points found as index coordinates, the horizontal and vertical pixel lengths of the same marked pixel are calculated, which are the pixel lengths of the horizontal and vertical directions of the individual stones, and the horizontal and vertical pixel lengths of all marked stone areas in the image are calculated by traversing all marked pixels in turn. The average pixel length of the horizontal and vertical distances of all the stones is calculated as the average pixel length of the stones in the image.

It should be noted that since the stone targets are closely connected and occluded from each other, there will be individual stone pixel regions with fewer and more pixel points and adherent stone pixel regions, i.e., white pixel regions with smaller regions in the binary image and white pixel regions with larger regions in the binary image, after the stone image prediction. The smaller or larger gravel pixel regions, which do not represent the real data of gravel, need to be discarded. According to the number of pixels of each gravel region recorded in the traversal pixel operation during gravel division, the 20% of the largest and the 20% of the smallest pixel region ranking in an image are subjected to the discard operation, and the final gravel pixel region obtained is the gravel region that can be used as the real value in the image.

V. Analysis of Experimental Results

A. The dataset

The object of this experiment is stone images, and since there is relatively little research on stone images and no public dataset to study, the stone images used in this experiment are all taken by webcam. There are a total of 40 stone images, and the labels contained in the 40 stone images have taken shape due to the number of stones in the captured images and the characteristics of tight adhesion.

In the deep learning training process, before the training of the stone images, data enhancement, which includes changing the brightness, image distortion, mirroring, rotation and other operations, so that the image becomes more diverse, the changed image into the neural network for training can improve the robustness of the network and reduce the impact of additional factors in various aspects on the segmentation[13]. After the above process, 40 stone images data can meet the experimental requirements.

The experimental shooting equipment is Hikvision webcam, model DS-IPC-B12V2-I. In order to ensure that the method of this experiment has high robustness, the shooting images are from stone samples under different light, different photos with different stone target sizes, different lighting conditions between photos, different colors of the stones themselves, and large differences between stone grain sizes.

B. The evaluation index

The experimental procedure of this experiment has stone segmentation as the main objective, and the study focuses on how to segment the stones in an effective operation. The ultimate goal of the experiment is to calculate the length of the effective particle size in the stone image. Therefore, the evaluation of the experimental results is divided into two parts: the evaluation of the accuracy of stone segmentation and the evaluation of the accuracy of stone particle size calculation.

The accuracy of semantic segmentation can be calculated using confusion matrix. As Table 2 shows the confusion matrix [14] calculation metrics.

TABLE II
Confusion_Matrix

Confusion_Matrix		**Predicted Class**	
		Positive	Negative
Actual Class	Positive	TP	FP
	Negative	FN	TN

The confusion matrix is the statistical classification result of the classification model, i.e., the number of samples that are classified correctly and wrongly, and then the result is displayed in a table. The figure 7 shows a schematic representation of the real and predicted labels in the confusion matrix.

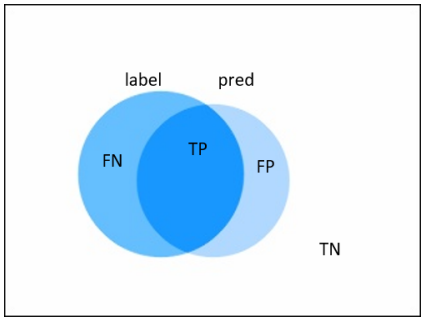

Fig. 7. Schematic representation of the true and predicted labels in the confusion matrix

The commonly used evaluation metrics for semantic segmentation are mIoU, mPA, Precision, and Recall.

- $mIoU$(Mean Intersection over Union)

In the semantic segmentation problem, the intersection-to-merge ratio (IoU) is the ratio of intersection and merge of the true label (ground truth) to the predicted segmentation of the class[15].

The $mIoU$ can be interpreted as the average intersection-to-merge ratio, i.e., the values of IoU are calculated on each class and then averaged.

$$IoU = \frac{TP}{TP + FP + FN} \tag{2}$$

$$mIoU = \frac{1}{k+1} \sum_{i=0}^{k} \frac{TP}{FN + FP + TP} \tag{3}$$

As Figure 8 shows the record of mIoU in training, the mIoU value on the test set is recorded once every 5 epochs of training.

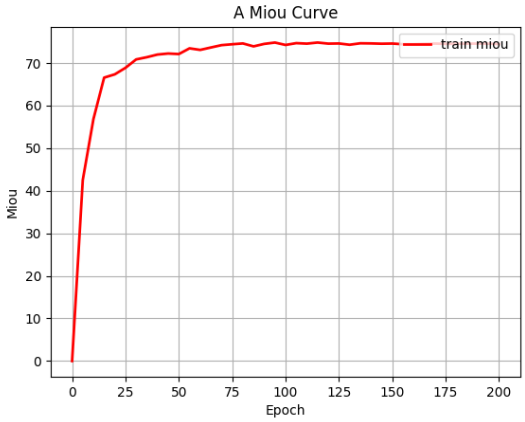

Fig. 8. The record of mIoU in training

As Figure 9 shows the values of mIoU calculated on the 8 test images after the training is finished, the weight file with the smallest Loss value is selected. Among them, the mIoU value reached 89% in the gravel region.

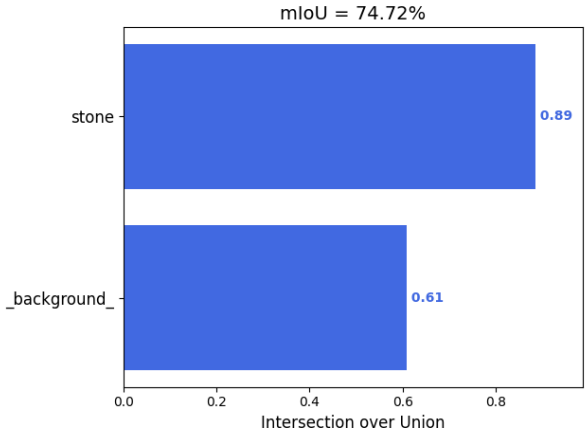

Fig. 9. Calculate the final mIoU value

- mPA(Mean Pixel Accuracy)

The ratio of the number of correctly classified pixels in each category to the number of all pixels in that category is calculated and then averaged.

$$PA = \frac{TP + TN}{TP + TN + FP + FN} \tag{4}$$

$$mPA = \frac{1}{k+1} \sum_{i=0}^{k} \frac{p_{ii}}{\sum_{j=0}^{k} p_{ij}} \tag{5}$$

The mPA values calculated on the eight test images at the end of training are shown in Figure 10, and the weight file with the smallest loss value was selected. Among them, the mPA value of the gravel area reaches 95%.

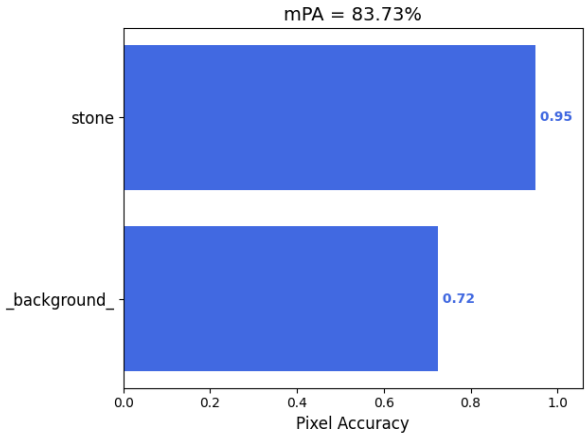

Fig. 10. Calculate the final mPA value

- Loss

The training Loss variation curve is illustrated in Figure 11.

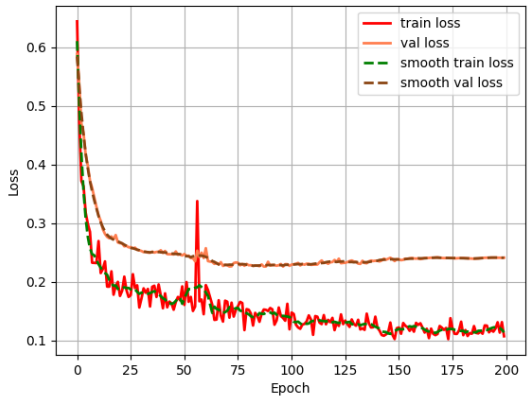

Fig. 11. The record of loss in training

- Calculation error

In terms of accuracy evaluation of sand and gravel particle size calculation, the calculation error is used to represent the error between the calculated results of sand and gravel particle size and the real results, in pixels. The calculation error is calculated as follows:

$$error = |image\_stone\_length - stone\_length| \tag{6}$$

Among them, image_stone_length represents the actual stone particle size length data (image_stone_length) calculated according to the stone particle size length in the picture, and stone_length is the real size of the actual stone particle size length (stone_length).

Among them, image_stone_length is automatically calculated after the end of the experiment, and the data form is the

actual sandstone particle size length calculated from the stone target pixel length. The actual particle length stone_length of stone is obtained by manual sampling measurement.

During manual measurement, measure the real stone particle size corresponding to the 40 collected stone sample test charts. Manually measure the sampled stone samples. Take the length calculated by four points on the upper, lower, left and right boundaries. Take the longest side of the rectangular area where the stone target is located as the longest particle size of the stone target. The average length of all the longest particle sizes is taken as the average length of the particle sizes in the picture.

C. Results analysis

In order to compare the segmentation accuracy of the segmentation model, the following experiments were conducted on the existing model. To ensure the fairness of the experiment, the backbone network was kept as VGG16, and the following experimental results were obtained.

Note that our dataset may not be applicable to all models. The results of the experiment are shown in table 3.

TABLE III
RESULTS BASED ON SEMANTIC SEGMENTATION OF STONE DATASET

Method	**Backbone**	**mIoU**	**mPA**	**mPrecision**
FCN	VGG16	60.18	70.34	75.32
HRNet	VGG16	66.49	76.47	81.06
DeepLabV3+	VGG16	70.23	78.54	83.67
PSPNet	VGG16	67.24	74.52	78.42
UNet(ours)	VGG16	73.12	81.37	86.58

Figure 12 shows the effect of network prediction of two pictures, the original picture, ground truth and predicted picture from left to right.

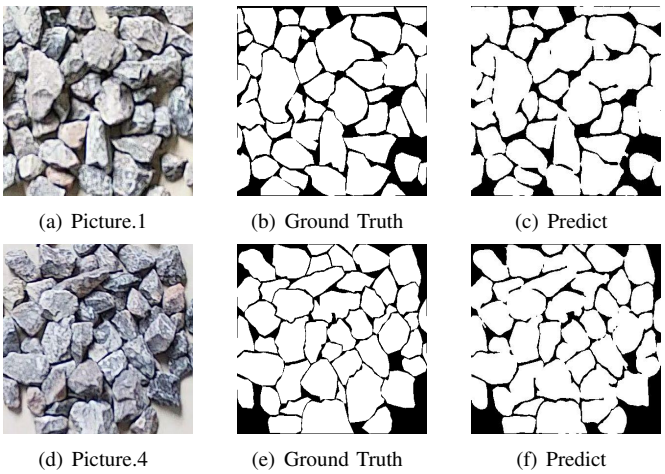

(a) Picture.1 (b) Ground Truth (c) Predict

(d) Picture.4 (e) Ground Truth (f) Predict

Fig. 12. Experimental effect picture

In terms of the effect of sand and gravel segmentation, after the completion of the experimental process, the stones in the current picture were measured manually, and the following results were finally obtained by comparing with the final calculated sand and gravel particle size, as shown in the table 4.

TABLE IV
STATISTICAL TABLE OF SAND AND STONE PARTICLE SIZE

Image number	Particle size calculated value(in pixels)	Calculate the value map length(In mm)	Particle size manually measured(in mm)	Calculation error(in millimeters)
1	31	12.4	13.3	0.9
2	28	11.3	12.5	1.2
3	38	15.2	18.3	3.1
4	42	16.8	19.3	2.5
5	45	18.0	21.2	3.2

VI. CONCLUSION

In this paper, a sand particle size detection system and method are proposed, which can quickly segment the sand target and accurately calculate the sand particle size.In sand target segmentation effect, using other traditional methods, after the split still have a lot of sand and gravel target individual adhesion together, and the innovation points of this paper is to first get the gravel image clipping, cutting to the smaller image size into the depth of learning network, do the adhesion area is less, for subsequent calculation length of sand particle size.After an image is clipped, it is divided into different individual images. After each calculation, the result of the clipped image is the calculation result of the original image.In terms of sand particle size calculation, the method of finding the coordinates of sand and stone is convenient and fast. Because the calculation accuracy is affected by the model segmentation, the degree of sand and stone adhesion, and the shooting environment, it can still be controlled within the acceptable range, and the calculation accuracy is relatively accurate.

ACKNOWLEDGMENT

The presented work is partially funded by the Natural Science Project of CQUST(Chongqing University of Science and Technology)(No.20220211), the Postgraduate Innovation Project of CQUST (No.CX2021021 and No.CX2021003). The authors would like to thank the anonymous reviewers for their valuable suggestions and comments.

REFERENCES

[1] K. Bhargavi, S. Jyothi, “A survey on threshold based segmentation technique in image processing”, International Journal of Innovative Research and Development, 2014, 3(12): 234-239.

[2] H. G. Kaganami and B. j. Zou , “Region-Based Segmentation versus Edge Detection”, 2009 Fifth International Conference on Intelligent Information Hiding and Multimedia Signal Processing, 2009, pp. 1217-1221.

[3] H. Lyu, H. Fu, X. Hu and L. Liu, “Esnet: Edge-Based Segmentation Network for Real-Time Semantic Segmentation in Traffic Scenes,” 2019 IEEE International Conference on Image Processing (ICIP), 2019, pp. 1855-1859.

[4] J. Long, E. Shelhamer, T. Darrell, “Fully convolutional networks for semantic segmentation”, Proceedings of the IEEE conference on computer vision and pattern recognition. 2015: 3431-3440.

[5] O. Ronneberger, P. Fischer, T. Brox, “U-net: Convolutional networks for biomedical image segmentation”, International Conference on Medical image computing and computer-assisted intervention, Springer, Cham, 2015: 234-241.

[6] H. Zhao, J. Shi, X. Qi, et al, “Pyramid scene parsing network”, Proceedings of the IEEE conference on computer vision and pattern recognition, 2017: 2881-2890.

[7] L. C. Chen, Y. Zhu, G. Papandreou, et al, “Encoder-decoder with atrous separable convolution for semantic image segmentation”, Proceedings of the European conference on computer vision (ECCV), 2018: 801-818.

[8] A. Krizhevsky, I. Sutskever, G. E. Hinton, “Imagenet classification with deep convolutional neural networks”, Communications of the ACM, 2017, 60(6): 84-90.

[9] D. Yu, H. Wang, P. Chen, et al, “Mixed pooling for convolutional neural networks”, International conference on rough sets and knowledge technology, Springer, Cham, 2014: 364-375.

[10] K. Simonyan, A. Zisserman, “Very deep convolutional networks for large-scale image recognition”, arXiv preprint arXiv:1409.1556, 2014.

[11] L. S. Huang, S. Shao, X. J. Lu, X. Y. Guo, J. C. Fan, “Multispectral image segmentation and alignment of lettuce based on convolutional neural network”, Journal of Agricultural Machinery, 2021, 52(09): 186-194.

[12] Y. Li, “Research on the detection and identification method of multiple types of lane lines”, Xi’an University of Petroleum, 2021.

[13] Y. Z. Zhang, “Research on target detection based on parameter-derived networks”, Heilongjiang University, 2021.

[14] H. G. Lewis, M. Brown, “A generalized confusion matrix for assessing area estimates from remotely sensed data”, International journal of remote sensing, 2001, 22(16): 3223-3235.

[15] H. S. Wang, L. Y. Cao, “Automatic Plant Leaf Segmentation and Phenotype Analysis Based on Full Convolutional Neural Network”, China Agricultural Chemistry News, 2021, 42(08): 161-168.

[16] N. Thein, H. A. Nugroho, T. B. Adji, and K. Hamamoto, “An image preprocessing method for kidney stone segmentation in CT scan images,” in 2018 International Conference on Computer Engineering, Network and Intelligent Multimedia (CENIM), 2018, pp. 147–150.

[17] Y. Ho and S. Wookey, “The real-world-weight cross-entropy loss function: Modeling the costs of mislabeling,” IEEE Access, vol. 8, pp. 4806–4813, 2019.

[18] R. Zhao et al., “Rethinking dice loss for medical image segmentation,” in 2020 IEEE International Conference on Data Mining (ICDM), 2020, pp. 851–860.

[19] H. Iyatomi et al., “An improved internet-based melanoma screening system with dermatologist-like tumor area extraction algorithm,” Computerized Medical Imaging and Graphics, vol. 32, no. 7, pp. 566–579, 2008.

[20] N. Grelier, “Maximum Clique in Generalisations of Disk Graphs and Plane Geometric Graphs on Degenerate Point Sets,” phdthesis, ETH Zurich, 2022.

[21] D. Q. Zhu, “Particle size detection of sandstone image based on deep learning”, Nanjing University of technology, 2020.

[22] S. Z. Xu, W. Liu, “Breast tumor cell image segmentation based on UNet networks”, Journal of electronic design engineering, 30 (12) : 63-66 + 73, 2022.

[23] W. L. Ding, C. Gu, M. K. Wang, et al., “Based on marginal prediction and marginal growth Image Segmentation Method”, High Technology Communications, 28(5) : 409-416, 2018.